Journal of Minerals and Materials Characterization and Engineering, 2020, 8, 27-46
https://www.scirp.org/journal/jmmce
ISSN Online: 2327-4085
ISSN Print: 2327-4077

Effect of Cu-Ni and Cu-Ni-Mn on the Microstructural and Mechanical Behaviour of As-Cast Non-Inoculated Hypereutectic Grey Iron

Seidu Ojo[1], Adama Sumaila[2], Onigbajumo Adetunji[3*]

[1]Department of Metallurgical and Materials Engineering, Federal University of Technology, Akure, Ondo State, Nigeria
[2]Ajaokuta Steel Company Limited (ASCO), Ajaokuta Complex, Kogi State, Nigeria
[3]School of Mechanical, Medical and Process Engineering, Queensland University of Technology, Brisbane, Australia
Email: *a.onigbajumo@qut.edu.au

How to cite this paper: Ojo, S., Sumaila, A. and Adetunji, O. (2020) Effect of Cu-Ni and Cu-Ni-Mn on the Microstructural and Mechanical Behaviour of As-Cast Non-Inoculated Hypereutectic Grey Iron. *Journal of Minerals and Materials Characterization and Engineering*, **8**, 27-46.
https://doi.org/10.4236/jmmce.2020.82003

Received: January 24, 2020
Accepted: March 17, 2020
Published: March 20, 2020

Abstract

The hypereutectic region of grey cast iron has received very little attention especially for designing cast products by researchers. Due to its high carbon equivalence, hypereutectic grey iron poses some challenges especially its tendency for grey to white transition (GWT) at this level of carbon content. However, hypereutectic grey iron possesses inherent properties that could be easily utilized for improved performance in automobile engines and brake pad system. Significantly, they could be modified for superior hardness, strength and toughness. This study presents the effect of microalloying on the mechanical behaviour of hypereutectic grey cast iron with carbon equivalence above 4.5. The first part of this work presented in this paper considers the addition of Cu-Ni and Cu-Ni-Mn to series of as-cast hypereutectic grey cast iron and their hardness and tensile strength were studied and compared. A total of 33 cast samples were obtained with the control sample. The examination of the micrographs revealed that graphite eutectics cells of Type A and A + D were obtained in the resulting microstructure. Results analyses showed that the ferrite forming tendency of silicon was suppressed due to the high carbon content of the as-cast hypereutectic grey iron coupled with the absence of inoculation which plays a great role in the graphite flake type, network, size and distribution. Cu-Ni microalloying was also confirmed to promote hardness with the hardening effect limit of nickel observed at 1.3% composition. For Cu-Mi-Mn addition, excess and free sulphur in the hypereutectic grey iron results in reverse effect of manganese on strength, hardness, reduced graphite flake size and shape.

Keywords

Hypereutectic Grey Iron, Microstructure, Hardness, Tensile Strength, Inoculation, Graphitization, Cast Iron, Alloying

1. Introduction

In grey cast iron, the carbon that exceeds the solubility in austenite precipitates as flake graphite [1]. According to Yin *et al*., 2001, grey irons usually contain 2.5% to 4% C, 1% to 3% Si, and additions of manganese, depending on the desired microstructure (as low as 0.1% Mn in ferritic grey iron and as high as 1.2% in pearlitic grey iron) [2]. Grey cast iron (GCI) having an excellent mechanical and friction properties has been the most renowned cast iron type especially for automobile engine systems as well as brake and clutch system of medium and heavy-duty carrying trucks [3]. In line with Angus 2013, the classification for alloyed irons has a wide range of base compositions with major additions of other elements, such as nickel, chromium, molybdenum or copper [4]. The basic strength and hardness of all iron alloys are provided by the metallic structures containing graphite [5]. The properties of the iron matrix can range from those of soft, low-carbon steel (18 ksi/124 MPa) to those of hardened, high-carbon steel (230 ksi/1586 MPa) [6]. The modulus of elasticity varies with the class of iron, shape (sphericity) and volume fraction of the graphite phase (percent free carbon) [6]. Because of their relatively high silicon content, cast irons inherently resist oxidation and corrosion by developing a tightly adhering oxide and subscale to repel further attack [7].

One reason for the wide use of iron castings is the high ratio of performance to cost that they offer. This high value results from many factors, one of which is the control of microstructure and properties that can be achieved in the as-cast condition [8]. This enabled a high percentage of ferritic and pearlitic iron castings to be produced without the extra cost of heat treatment [9] [10]. However, producing high quality castings (in as-cast condition) requires the use of consistent charge materials, and the implementation of consistent and effective practices for melting, holding, treating, inoculation and cooling in the mould [10]. Heat treatment is a valuable and versatile tool for extending both the consistency and range of properties of iron castings beyond the limits of those produced in the as-cast condition [10].

Interestingly, the microstructural base of GCI can be modified by the addition of alloying elements as well as heat treatment to induce desired properties [11]. The heat treatment route, however, is quite limited to the initial microstructural and alloying additives during the casting operation. In most cases, these approaches usually entail increased production and finishing cost of the cast product [12]. Microstructural modification using alloying additives remains the most economical and optimal approach to inducing desired properties in the base

GCI [13]. Alloying additions would be such as to improve mechanical properties especially the wear resistance of the cast iron for enhanced service life, reduce maintenance and warranty cost [14].

The amount and type of alloying element in grey cast iron influence its material response to service application. While hypoeutectic and slightly hypereutectic grey iron has been widely explored, strong hypereutectic compositions remains a region of grey iron eutectics that is hardly explored by researchers. Previous research had shown effort in exploring the possibility of hypereutectic grey iron for brake disc application [15] [16] [17]. Most studies in grey cast iron alloy had focused on hypoeutectic composition [18]-[26] and very rare study have considered the behaviour of grey iron at slightly hypereutectic composition [3] [11]. Hypereutectic grey iron beyond chemical equivalence of 4.5 is generally regarded as unpliable to mechanical applications [27]. This research investigates a novel approach to the production of hypereutectic grey iron in the absence of traditional inoculation. To the researcher's knowledge, there are no investigations on the microalloying of Cu-Ni and Cu-Ni-Mn to the addition of hypereutectic grey cast iron in the absence of traditional inoculation. The study therefore seeks to find out the influence of Cu-Ni and Cu-Ni-Mn on the hardness and tensile properties of a developed hypereutectic GCI (chemical equivalence = 4.5 - 5.2 wt%) composition for improved performance in mechanical properties and compare with typical grey iron and slightly inoculated hypereutectic grey iron in relevant studies.

2. Materials and Experimental Procedure

Hypereutectic grey iron was obtained by melting base grey cast iron of engine block scrap 3.9 - 4.0 wt% CE (3.2 - 3.3 wt% C, 2.2 - 2.3 wt% Si, 0.4 - 0.5 wt% Mn, 0.1 - 0.12 wt% P and 0.03 - 0.05 wt% S) in a cupola furnace. The melting was critically conditioned for casting without inoculation to investigate graphite nucleation and resulting properties of the hypereutectic grey iron without the inoculant. Cupola furnace route was used as a cheap source of hypereutectic iron production by cheap carbon pick up resulting from the coal-iron interaction. Ladle addition was employed for Copper (99.9%) in the form of particle chips, FeNi (75 wt% Ni) and FeMn (82 wt% Mn) in particulate form in line with similar investigation in previous study. The experimental heats were superheated to 1560˚C and maintained for 5 minutes.

The test castings were poured at 1470˚C upon the addition of the ferro alloy and copper additive. Cu additions were varied from 1.5 - 2.4 wt% across the sample alloy series and Ni was varied between 3.0 - 4.5 wt% within the sample alloy series for the first 16 alloy sample (**Table 1**). The last 16 alloy samples obtained had Cu varied between 0.5 - 1.4 wt% across the alloy series while Ni and Mn were varied from 0.6 - 1.5 wt% and 0.5 - 1.1 wt% respectively within the alloy series (**Table 1**). Round test bar samples (20 mm diameter, 160 mm length) were gated off the cooled casting.

Table 1. Composition and chemical equivalence of alloys studied.

Sample	C	Si	Mn	P	S	Cu	Ni	Cr	Fe	CE
Base Scrap	3.24	2.25	0.42	0.099	0.03	0.075	0.065	0.21	93.8	3.9924
1	4.33	1.2	0.328	0.0781	0.1082	0.348	1.06	0.117	91.5	4.76171
2	4.17	1.38	0.39	0.0603	0.0694	0.318	1.16	0.104	91.8	4.6483
3	4.35	1.17	0.368	0.0755	0.109	0.441	1.45	0.106	91.2	4.77207
4	4.03	1.33	0.334	0.0757	0.0788	0.548	1.48	0.11	91.3	4.4949
5	4.32	1.6	0.418	0.066	0.325	0.867	2.28	0.183	89.5	4.95525
6	4.35	1.63	0.361	0.0762	0.20791	0.624	1.1	0.126	91.1	4.95651
7	4.32	1.48	0.364	0.124	0.097	0.866	0.68	0.148	91.2	4.84041
8	3.78	1.16	0.32	0.105	0.0757	0.44	1.402	0.122	92.9	4.18778
9	4.35	1.45	0.247	0.0771	0.1861	0.534	1.05	0.0864	91.4	4.88991
10	3.9	2.14	0.273	0.067	0.182	0.978	1.37	0.106	90.8	4.66626
11	3.97	1.55	0.311	0.0617	0.1754	0.526	0.876	0.551	92	4.53938
12	4.35	1.24	0.427	0.0591	0.173	0.415	0.645	0.0517	92.1	4.81629
13	4.03	1.51	0.233	0.0817	0.179	0.628	1.2	0.4599	91.4	4.58737
14	4.04	1.65	0.267	0.078	0.314	1.18	1.65	0.0921	90.5	4.68812
15	4.28	2.04	0.345	0.167	0.317	0.32	1.07	0.0702	92.1	5.05781
16	4.18	2.04	0.369	0.128	0.276	0.648	0.696	0.0903	91.4	4.94428
17	4.35	1.18	0.57	0.124	0.088	0.39	0.343	0.0465	92.4	4.76844
18	4.35	1.18	0.522	0.123	0.262	0.488	0.724	0.0455	92.5	4.82586
19	4.35	1.33	0.469	0.107	0.269	0.492	0.253	0.0454	92.4	4.87767
20	4.15	2.01	0.508	0.0859	0.308	0.446	0.181	0.0608	92.3	4.91494
21	4.35	1.38	0.776	0.0931	0.39	0.369	0.553	0.0341	91.5	4.9341
22	3.92	1.16	0.458	0.0699	0.076	0.206	0.253	0.029	93.2	4.32788
23	4.35	1.47	0.582	0.11	0.2892	0.498	0.41	0.039	91.8	4.93054
24	4.17	2.19	0.761	0.0868	0.304	0.365	0.266	0.0601	91.6	4.99302
25	4.35	1.3	0.734	0.109	0.293	0.466	0.742	0.0401	91.3	4.87569
26	4.35	1.35	0.576	0.099	0.244	0.39	0.417	0.0405	91.9	4.87602
27	4.35	1.37	0.541	0.102	0.0832	0.424	0.279	0.047	92.1	4.82956
28	4.35	1.46	0.593	0.0992	0.101	0.512	0.231	0.0466	91.9	4.86513
29	4.15	1.3	0.734	0.0984	0.0955	0.645	0.758	0.0464	91.5	4.61052
30	4.35	1.31	0.675	0.0952	0.133	0.638	0.535	0.044	91.5	4.82619
31	3.94	2.07	0.663	0.105	0.302	0.774	0.435	0.0756	91.3	4.72276
32	4.03	2.11	0.593	0.0879	0.308	0.756	0.456	0.0718	91.6	4.82794

*CE = Carbon Equivalence (CE) = $\text{Total\%C} + \frac{1}{3}(\%\text{Si} + \%\text{P})$ Singh 2010.

The effects of additives were analysed by comparing microstructures (graphite, carbide, inclusion) of the hypereutectic irons treated with varying amounts of Cu-Ni and Cu-Ni-Mn.

The tensile tests were performed on the samples produced using the Universal Testing Machine (instron 3369). The samples for the test were machined to round specimen having the following configuration of 6 mm grip diameter, 10 mm grip length, 4 mm gauge diameter and 30 mm gauge length. The test was carried out at room temperature using an Instron universal testing machine operated at a strain rate of 10^{-3}/s. The tensile characteristics evaluated from the tension test are the ultimate tensile strength. Two tests were performed from each composition of the samples produced to ensure reliability of the data generated. The broken pieces are taken away from the machine and type of fracture is noted. By fitting the broken pieces together, final length (gauge length at failure) of the specimen and final diameter at the neck (diameter at failure) were recorded.

The optical emission spectrometry was carried out using the Spectro-Lab XG-8 (Ametec) Metal Analyzer. This test method covers the routine control analysis in iron and steelmaking operations and the analysis of processed material. It is designed for chill-cast, rolled, and forged specimens. Better performance is expected when reference materials and specimens are of similar metallurgical condition and composition. However, it is not required for all applications of this standard.

Microstructural analysis was carried out using the as-cast alloy specimen obtained from the ingot. Unetched microstructure was used to compare the graphite flake morphology using the AFS chart × 100 with five different fields selected for quantitiative estimation of phase component. The samples were etched using 2% Nital before the microstructural investigation was carried out. Image analysis was carried out to obtain various phase characteristics with an average of four fields taken with an image analyzer for accuracy.

Hardness tests (HRC) were carried out on the samples produced using Digital Rockwell Hardness Testing Machine. The sample's surfaces were well-grinded inaccordance to standard metallographic procedures to ensure that a smooth surface is produced and to allow for reliable measurement of the hardness values. Multiple hardness tests were performed on each sample and the average from the values was taken as the hardness value of the specimen.

3. Results and Discussion

3.1. Chemical Analysis

The chemical composition of the alloys produced is listed in Table 1. The base alloy is a typical cast under traditional use while the alloyed grey iron is compiled in series A (1 to 4) and B (1 to 4) with respect to Cu-Ni variations across A series and Cu-Ni-Mn variations across B series (Table 2). The use of cupola furnace was justified with the production of cast alloy as slightly hypereutectic

Table 2. Cu-Ni and Cu-Ni-Mn weight percent addition to cast metal in the ladle.

Series Identity	Sample Number	Varied Weight % Additives
Alloy series A1	Sample 1	1.5% Cu, 4.5% Ni Modified GCI
	Sample 2	1.5% Cu, 4.0% Ni Modified GCI
	Sample 3	1.5% Cu, 3.5% Ni Modified GCI
	Sample 4	1.5% Cu, 3.0% Ni Modified GCI
Alloy series A2	Sample 5	1.8% Cu, 4.5% Ni Modified GCI
	Sample 6	1.8% Cu, 4.0% Ni Modified GCI
	Sample 7	1.8% Cu, 3.5% Ni Modified GCI
	Sample 8	1.8% Cu, 3.0% Ni Modified GCI
Alloy series A3	Sample 9	2.1% Cu, 4.5% Ni Modified GCI
	Sample 10	2.1% Cu, 4.0% Ni Modified GCI
	Sample 11	2.1% Cu, 3.5% Ni Modified GCI
	Sample 12	2.1% Cu, 3.0% Ni Modified GCI
Alloy series A4	Sample 13	2.4% Cu, 4.5% Ni Modified GCI
	Sample 14	2.4% Cu, 4.0% Ni Modified GCI
	Sample 15	2.4% Cu, 3.5% Ni Modified GCI
	Sample 16	2.4% Cu, 3.0% Ni Modified GCI
Alloy series B1	Sample 17	0.5% Cu, 1.5% Ni, 1.1% Mn Modified GCI
	Sample 18	0.5% Cu, 1.2% Ni, 0.9% Mn Modified GCI
	Sample 19	0.5% Cu, 0.9% Ni, 0.7% Mn Modified GCI
	Sample 20	0.5% Cu, 0.6% Ni, 0.5% Mn Modified GCI
Alloy series B2	Sample 21	0.8% Cu, 1.5% Ni, 1.1%Mn Modified GCI
	Sample 22	0.8% Cu, 1.2% Ni, 0.9% Mn Modified GCI
	Sample 23	0.8% Cu, 0.9% Ni, 0.7% Mn Modified GCI
	Sample 24	0.8% Cu, 0.6% Ni, 0.5% Mn Modified GCI
Alloy series B3	Sample 25	1.1% Cu, 1.5% Ni, 1.1% Mn Modified GCI
	Sample 26	1.1% Cu, 1.2% Ni, 0.9% Mn Modified GCI
	Sample 27	1.1% Cu, 0.9% Ni, 0.7% Mn Modified GCI
	Sample 28	1.1% Cu, 0.6% Ni, 0.5% Mn Modified GCI
Alloy series B4	Sample 29	1.4% Cu, 1.5% Ni, 1.1% Mn Modified GCI
	Sample 30	1.4% Cu, 1.2% Ni, 0.9% Mn Modified GCI
	Sample 31	1.4% Cu, 0.9% Ni, 0.7% Mn Modified GCI
	Sample 32	1.4% Cu, 0.6% Ni, 0.5% Mn Modified GCI

carbon compositions with high carbon equivalence and carbon content ranging from 3.9% to 4.35% for all the alloys produced. High carbon content of the produced hypereutectic GCI is expected to restrain the forming tendency of silicon as suggested in [3] [26]. The sulphur content of the base scrap reveals 0.03%

while the as-cast alloys range between 0.069% and 0.402% as presented in the chemical composition results of the produced alloys. Relative to the manganese content of the base scrap, the chemistry across the as-cast GCI alloy implies manganese loss. Hence, the presence of high sulphur the manganese content of the GCI will be assessed and fixed as MnS in line with Gundlach, 2014 [28]. Effect of manganese in the chemistry of the alloy was also pronounced upon the addition of ferromanganese in series B (1 to 4), which was lost due to manganese oxidation in the furnace when compared to cast alloy in series A (1 to 4). This oxidation loss of manganese is also confirmed by comparing the manganese content of the base scrap of 0.42% before the furnace melting with the produced alloy which ranged between 0.23% and 0.4% series A and the addition of manganese with which alloy series B ranged between 0.458% - 0.78%.

3.2. Microstructural and Mechanical Behaviour

In order to evaluate the graphite flakes morphology, the AFS chart was used to make needed comparison at 20 μm at ×100 magnification. The microstructures (100 μm) are presented in **Figure 1**. The additions are in two categories: nickel and copper addition in the A series at 40% - 60% initial weight percent reduction in copper, 30% - 60% reduction in nickel. Series B had the addition of copper and nickel using the same initial weight reduction in percentage addition as series A with manganese addition for alloy 45% - 80% initial weight percent reduction as shown in **Table 2**. These additions are in the purview and range of copper, nickel and manganese addition to grey cast iron from previous research effort [28] [29] [30]. Modifications done in this research are based on hypothetical fine tune to re-access possible outcome upon the iterations of the addition of these alloying elements especially with the use of a cupola furnace which is usually avoided by researchers [31].

The A series alloy (sample 1 - 16) reveals type A graphite morphology (etched microstructure) in a fully pearlitic matrix. Predominantly, alloy 3 and 4 (series A1), 8, (series A2) and 10 (series A3), reveals a combined formation of the type A graphite with a resulting undercooled type D graphite. The graphite phase formation outlining the dendritic structure of the matrix (10% - 25%) is observed to be in line with the established research investigations in literatures [27] [32] [33] [34]. The graphite flake size ranged from 4A to 5A with sizes predominantly between 25 mm to 3000 μm [35].

Within the addition of manganese and reduction in the weight percent of nickel and copper for the B series alloy, type D graphite (40% - 55%) was obtained for most of the as-cast ingot with the presence of type A graphite. As expected, the metal matrix was fully pearlitic with graphite flake size ranged from 6A to 8A with sizes predominantly between 3000 μm to 1500 μm (series B) (**Figure 1**). The predominance of Type D graphite in series B alloys confirms that the solidification range of the non-inoculated grey iron with reduced addition of copper and nickel as graphitizers, resulted into higher degree of undercooling and fewer eutectic cells in agreement with the findings of Fras and Gorny, 2012

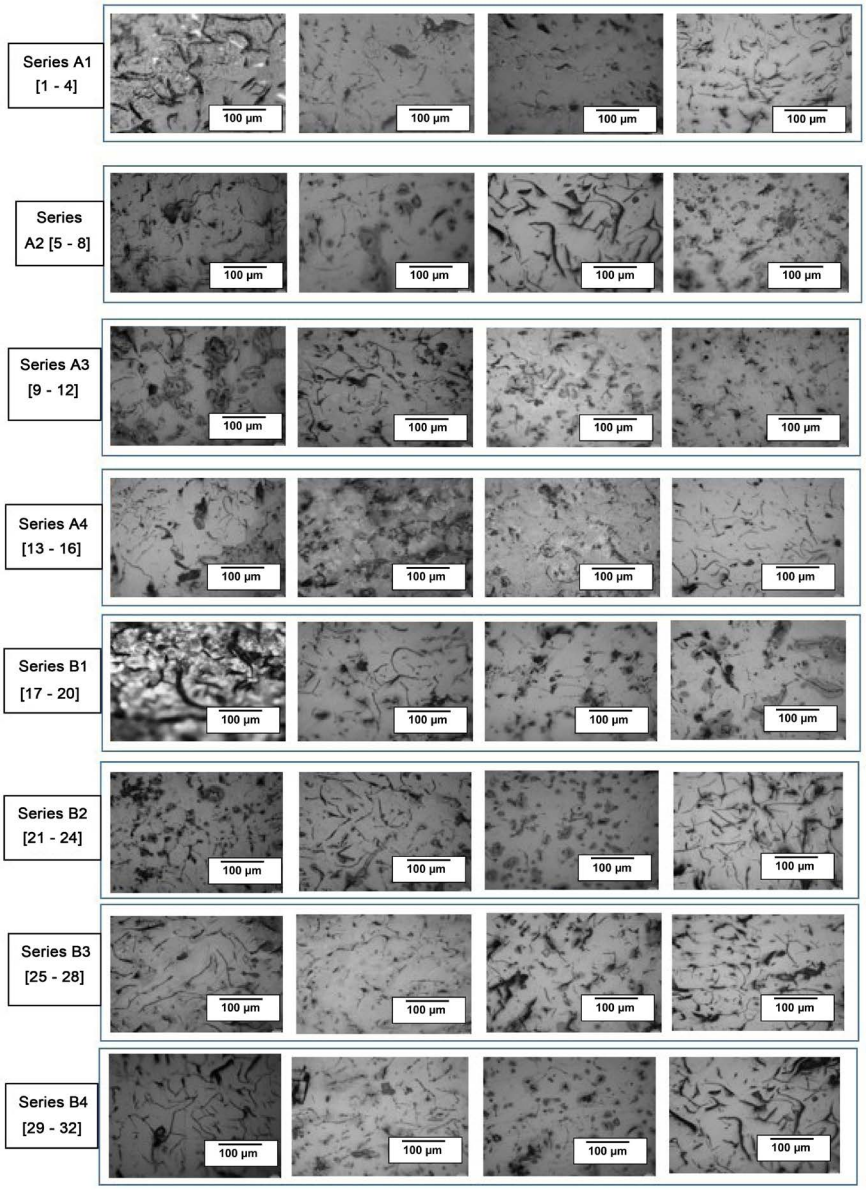

Figure 1. Etched microstructure of various alloys produced in the study, identified as 1) series A1, A2, A4 and A4 (Cu-Ni addition), 2) series B1, B2, B3 and B4 (Cu-Ni-Mn addition).

[34]. This also suggests that the eutectic cell growth rate and free energy eutectics of D type graphite transformation is below the range of type A graphite [36].

The microstructures of alloy 20 (series B1), 21 and 22 (series B2), 25 (series B3), 31 and 32 (series B4) confirms the presence of manganese sulphide (MnS) in the matrix of the as-polished specimens with uniform distribution around the proeutectic dendrites in tandem with the report of Gundlach *et al*., 2015 and Vadiraj *et al.,* 2010 [3] [26]. This observation is largely attributed to the increased composition of manganese and sulphur in these alloys. Higher combination of Mn and S, which usually result in MnS inclusions in a uniform distribution within the GCI matrix had been reported by Alderson 1983 [37]. The solu-

bility of S and MnS are a function of the percentage weight composition of S and Mn content in the melt and the microalloying temperature. Therefore, increasing manganese content and decreasing temperature decreases the solubility of sulphur in the grey iron. The solubility limit of MnS in grey iron is suggested between 0.03 - 0.045 which was obtained as [(%Mn × %S) + 0.3)] [26] [37]. This implies that if the MnS concentration is above the solubility limit of the cast iron, MnS will precipitate from the melt prior to reaching the eutectic temperature.

Since conventional GCI production is by-passed due to non-inoculation in this study, the solidification of the produced alloy is better analysed using the theory of recalescence. During cooling of the melt from the liquidus, an initial low temperature is reached below the equilibrium temperature caused by undercooling [27]. Once solidification begins, there is a release of thermal energy, which raises the temperature of the cooling melt to the steady solidification temperature, which is referred to as recalescence. The amount of recalescence indicates the effectiveness of inoculation [27] [38]. Since the presence of inoculant promotes more eutectic nucleus to be formed thereby forcing undercooling to becoming rapid, the resulting grey iron microstructure is formed around the graphite eutectic temperature. Prolonged undercooling would result in more primary austenite to nucleate at the expense of eutectic graphite during solidification [27] [32]. In the absence of graphite formers such undercooling results in the carbide eutectic equilibrium, resulting in white cast iron [27] [28] In the presence of graphitizers like copper and nickel such as added in this study, recalescence after reduced undercooling will result in matrix with type A graphite [39]. This occurrence is as a result of cell growth decrease with increased interfacial distance during solidification [36]. The critical growth rate of cells will correspond to the transformation number of cells at the eutectic. Adequate inoculation or graphitizing element increases the number of cells leading to the primary austenite transformation from the cementite eutectic (CE) into type D + CE and then type D graphite and then type D and A graphite and finally type A graphite [36].

This transformation analysis helps to understand the reason why type D graphite was present in the matrix of alloy series A (3, 4, 8 and 10) microstructure in fewer amounts and predominant in alloy series B which correlates with the weight addition of copper and nickel acting as graphitizers in series A and B grey iron produced. Furthermore, the sulphur intake into the alloy system by the reason of the furnace is considered to have influenced the type A and D mixture as noticed in the microstructure of the alloy produced in accordance with [36].

The Type D graphite which is defined by the small distances between the graphite flakes as a result of carbon diffusion path in the austenite between the graphite flakes during eutectoid transformation favours the formation of ferrite. As such one would have expected ferrite/pearlite matrix in the produced alloy series A and B, however, high CE value with the increased presence of copper [4] [36] suppresses ferritic formation with the presence of type D graphite.

3.2.1. Hardness

The average hardness value of three indentations on the alloy samples is presented in Table 3. The variation in hardness relative to the variation in Cu-Ni and Cu-Ni-Mn addition is shown in Figure 2. The hardness values of the alloys produced were in the range of 354 - 513 HV (Vicker's hardness) for alloy series

Table 3. Mechanical properties for the produced alloys.

Sample	Ultimate Tensile Strength (UTS)—MPa	Modulus (E)—MPa	Max. Extension at UTS (mm)	Hardness (VH)
Base alloy	226	188,857.25	0.71	241
1	227.39	23,258.98	0.483	412
2	233.98	26,591.76	0.484	434
3	256.34	22,436.65	0.6	402
4	269.21	24,306.08	0.62	458
5	195.62	21,920.02	0.79	458
6	208.21	21,043.17	0.53	423
7	245.83	20,919.35	1.31	354
8	262.47	20,342.65	1.35	471
9	218.30	15,037.89	2.62	458
10	281.11	19,991.65	0.74	513
11	230.71	15,256.17	0.63	498
12	223.86	18,976.56	0.45	484
13	213.77	17,788.58	0.51	458
14	145.65	13,245.32	0.039	434
15	169.89	14,898.58	1.59	354
16	200.18	20,649	0.47	458
17	226.72	18,859.83	0.72	354
18	186.35	18,082.91	0.54	372
19	179.84	20,655.68	0.46	363
20	168.0	23,254.84	0.4	336
21	111.99	18,472.36	0.44	318
22	230	23,463.87	0.52	310
23	157.36	21,572.99	0.05	327
24	186.83	24,010.95	0.049	318
25	173.18	19,597.46	0.47	382
26	150.57	22,225.90	0.42	266
27	217.43	24,306.94	0.51	279
28	213.90	24,762.38	0.63	336
29	239.59	21,078.47	0.64	382
30	231.45	20,195.65	0.62	336
31	223.25	20,051.78	0.61	345
32	178.61	20,472.81	0.62	363

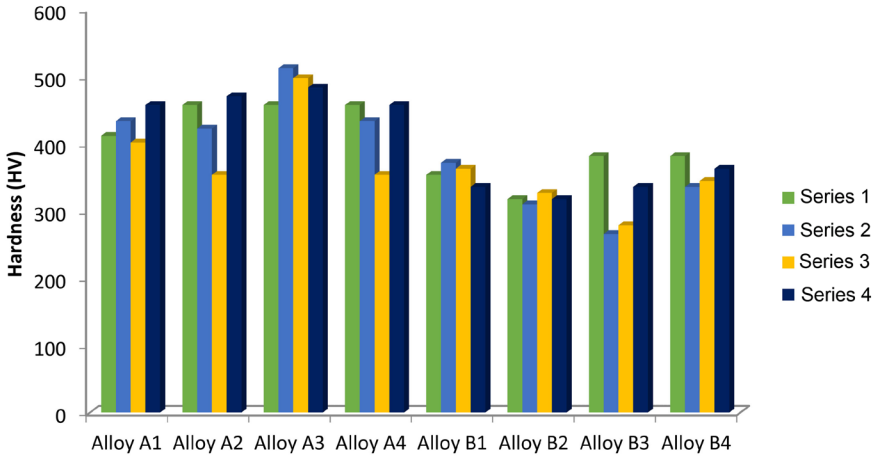

Figure 2. Comparison between the Hardness of the produced alloys. [A-Alloy: A1—1.5% Cu, A2—1.8% Cu, A3—2.1% Cu, A4—2.4% Cu]; [A-Alloy Series—Series 1: 4.5% Ni, Series 2: 4% Ni, Series 3: 3.4% Ni, Series 4: 3% Ni]; [B-Alloy: B1—0.5% Cu, B2—0.8% Cu, B3—1.1% Cu, B4—1.4% Cu]; [B-Alloy Series—Series 1: 1.5% Ni - 1.1% Mn, Series 2: 1.2% Ni - 0.9% Mn, Series 3: 0.9% Ni - 0.7% Mn, Series 4: 0.6% Ni - 0.5% Mn].

A with alloy 8 (series A2), 10, 11 and 12 (series A3) performing best. Alloy series B results in hardness value between 266 and 382 with alloy 18 (series B1), 25 (series B3) and 29 (series B4) ranking highest. The high hardness generally obtained in both series compared to the base alloy could be attributed to the solid solution strengthening associated with the pearlitic matrix as reported by Vadiraj *et al.,* 2010 [3]. While increased carbon content (high carbon equivalence) and the absence of inoculation suppresses the formation of ferrite/pearlite matrix [3] [15] the increased copper content promotes pearlite formation [35] which justifies the increased hardness value generally observed across the alloy produced. Hardness is also observed to increase with more copper addition in line with [29] as shown in **Figure 3**. The increased level of hardness in alloy 1 - 16 (series A) compared to 17 - 32 (series B) when compared with the study of Vadiraj et al., 2010 suggest the hardening effect of nickel in grey iron which increases with nickel addition until it reaches its limit [3] [37]. Hardening effect of nickel (**Figure 4**) is observed to have increased beyond the 1.2% - 1.5% concentration mark of nickel in the alloy suggesting the possible formation of bainite in thin sections of the cast, also in line with the findings of Ruff and Wallace [35].

Alloy 8, 10, 11 and 12 in series A reveals the presence of intercellular carbide distributed along the eutectic boundaries. This probably explains the reason for their improved hardness compared to other alloys in the A and B series. The carbide along the eutectic boundaries (white phases) are much harder (750 - 1000 HV) according to [3] [26] compared to the influence of pearlite matrix adding to the hardness of the alloys. The intercellular carbide formation in the alloy is also associated with phosphide eutectic in the presence of lower manganese content with high sulphur concentration [32] [37] [39]. At higher manganese level in the alloy 17 - 32 (series B), carbides were not visible even at higher sulphur levels. Intercellular carbide resulting from phosphide eutectic as a result

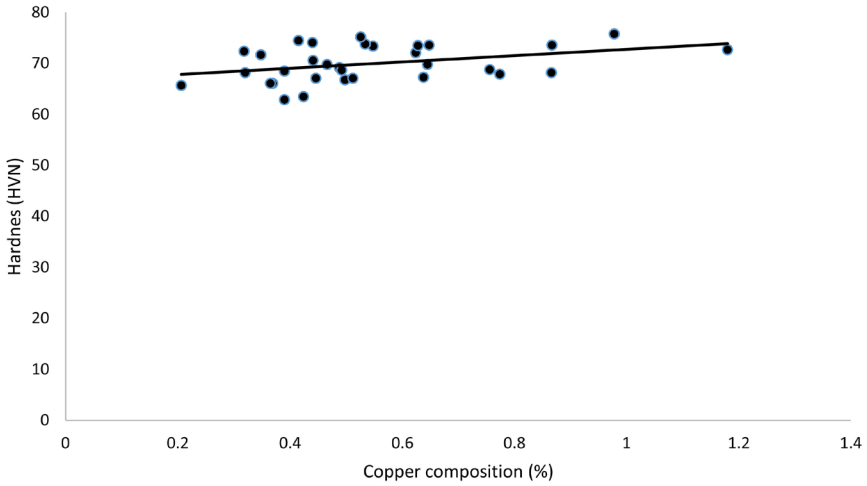

Figure 3. Effect of copper on the trend of hardness property indicating increasing hardness with increased copper.

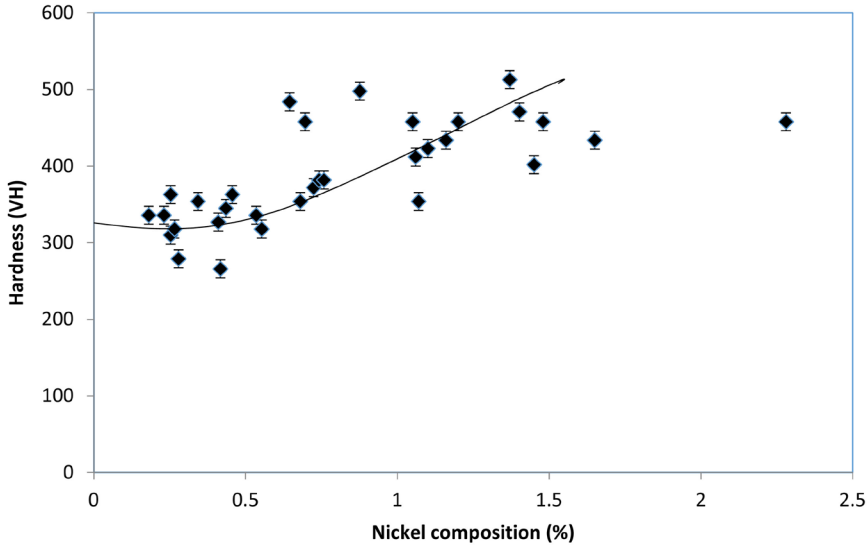

Figure 4. Effect of percentage nickel addition on the trend of hardness property indicating increasing hardness with nickel addition until about 1.5% limit of effect.

of manganese is no longer sufficient to buffer the free sulphur concentration available in the alloy system. Gundlach *et al*., 2015 suggested that when free sulphur is held within the domain of 0.10% at higher manganese content, intercellular carbides will be prevented which was in agreement with the observation of the result and the non-presence of intercellular carbide in alloy 17 - 32 (series B) (**Figure 5**). Excess manganese beyond that required to fix sulphur has the tendency to promote pearlite formation and eliminate free ferrite and consequently hardness [28] [37]. The hardness value was expected to rise due to the increase in the manganese content alloy 17 - 32 (series B) in line with Vadiraj *et al.,* 2010 findings [3] but this was not the case. **Figure 5** shows a plot using the relation between hardness and excess sulphur adapted from the approach of Mampaey and Gundlach [39]. The excess sulphur-hardness relationship obtained agrees

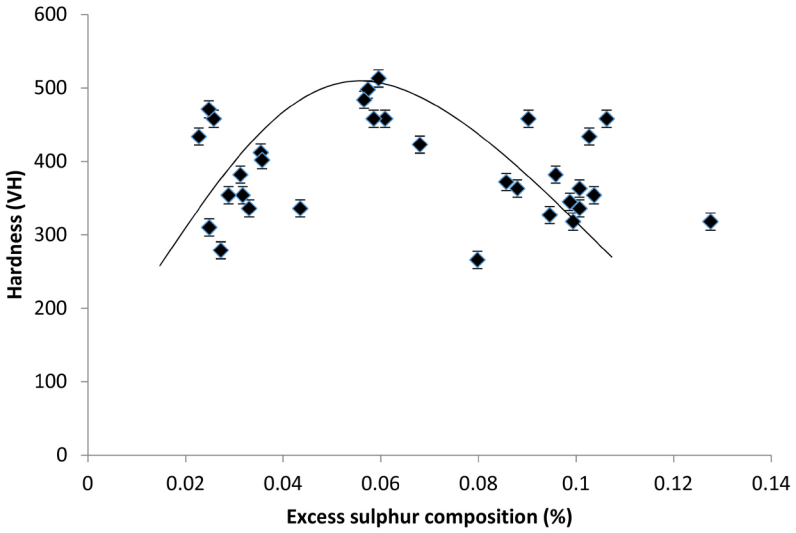

Figure 5. Effect of excess Sulphur on the hardness properties of the produced alloy with hardness level reducing at the domain of 0.05 sulphur content.

with the study and results of Alderson [37] with which manganese addition increases as a function of the sulphur content in the alloy. Alderson stated that the addition of manganese yielding desired hardness in the presence of sulphur is a function of the relation Mn < (1.7 * S), where Mn and S are the compositions of manganese and sulphur in the melt. In other words, when the total weight composition of manganese is greater than 1.7 times the weight composition of sulphur, expected hardness begins to decline [37].

In accordance with SAE J431 and ASTM A-438, extra heavy-duty service brake drums and clutch plates (G11H21 c) are required to have 225 HV (214 HB) - 236 HV (224 HB). This is close to the hardness value of grey iron pressure plate used by Vadiraj *et al.,* 2010 as the control alloy having 241 HV (229 HB) [3]. The hardness value of the alloys produced in this study has between one-half to two times that which is obtainable from specified grey iron for brake disc usage. This is expected to have an associative effect on the wear properties of the alloy produced, which could be considered in further study.

3.2.2. Tensile Strength

The results of the tensile strength property of the cast alloy are shown in **Table 3**. The ultimate tensile strength (UTS) for alloy in series A (1 - 16) shows values generally between 145 - 281 MPa and 111 - 239 MPa for alloy in series B (17 - 32). Alloy 3 (256 MPa), 4 (269 MPa), 8 (262 MPa) and 10 (281 MPa) were observed to give the highest strength. The comparison between the alloy series is shown in **Figure 6**. A fully pearlitic matrix in the microstructure of the alloy 3, 4, 8 and 10 (series A) (**Figure 1**), suggests the incidence of the high strength that was observed in these alloys [35].

The increased strength in alloy 3, 4, 8 and 10 when compared with the average UTS value observed for other alloys tend to increase with the value of percentage nickel content in the GCI as shown in **Figure 7**. This observation is consistent with

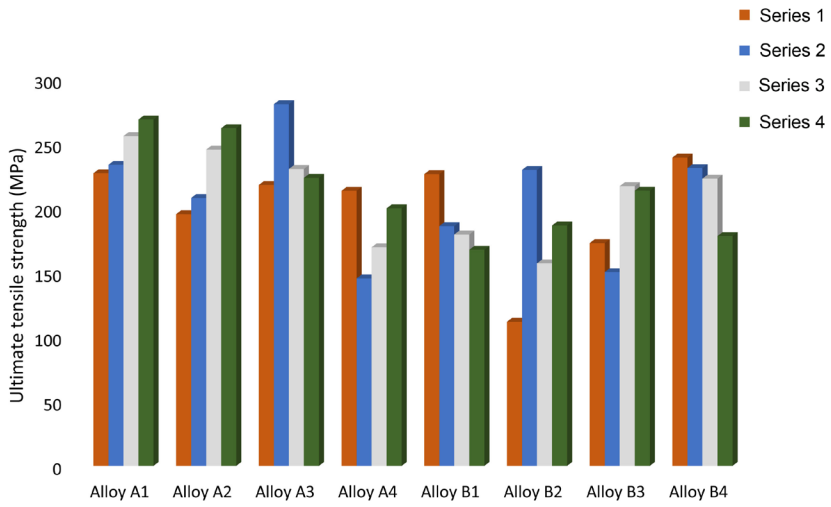

Figure 6. Comparison of ultimate tensile strength across the alloys produced [A-Alloy: A1—1.5% Cu, A2—1.8% Cu, A3—2.1% Cu, A4—2.4% Cu]. [A-Alloy Series—Series 1: 4.5% Ni, Series 2: 4% Ni, Series 3: 3.4% Ni, Series 4: 3% Ni]; [B-Alloy: B1—0.5% Cu, B2—0.8% Cu, B3—1.1% Cu, B4—1.4% Cu]; [B-Alloy Series—Series 1: 1.5% Ni - 1.1% Mn, Series 2: 1.2% Ni - 0.9% Mn, Series 3: 0.9% Ni - 0.7% Mn, Series 4: 0.6% Ni - 0.5% Mn].

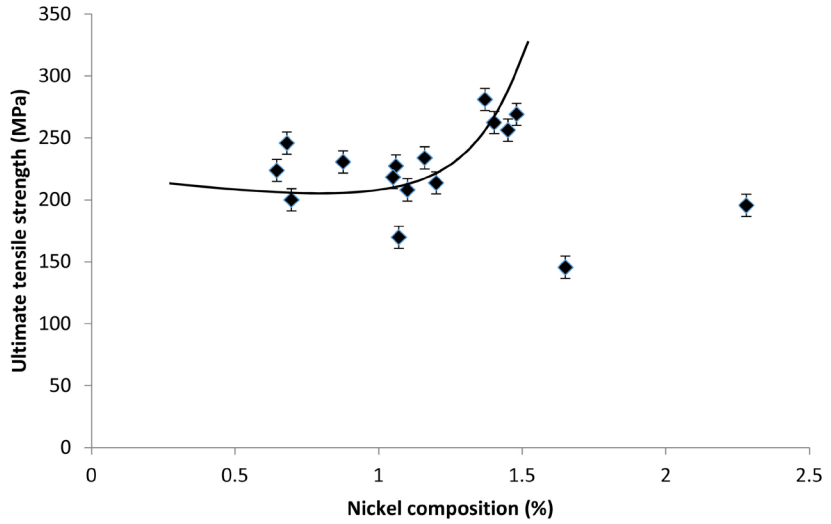

Figure 7. Influence of Nickel addition on the ultimate tensile strength.

the behaviour of nickel addition to grey iron in previous studies and theories [29] [32] [35]. A plot of nickel addition with UTS in **Figure 7** shows that nickel increased the ultimate tensile strength until about 1.5% in the grey iron. UTS after this percentage content of nickel decreased further. This response is a function of the grain refining effect of nickel addition [29] [32], having reached its peak at this point and further addition does not have much effect on the strength of the alloy.

Increasing the manganese content in the alloy series (17 - 32) was targeted at promoting pearlite formation and further improving the strength and hardness of the alloy. The result, however, was not as expected, as the UTS reduced more

in this alloy series. From the analysis of the microstructure, the presence of increased sulphur and manganese sulphide inclusion beyond solubility limit in the microstructure had an adverse effect on the strength. Figure 8 shows the relationship between percentage sulphur content and ultimate tensile strength in the grey iron. In Figure 9, the relationship between the solubility limit of MnS in grey iron and the strength suggests that higher strength is obtainable at lower sulphur content for a given percentage composition of manganese [3]. The observed behaviour of the grey iron to the increment in sulphur content as well as the solubility limit of MnS is in good standing with the findings of Gundlach *et al*., 2015 [27] and Alderson, 1983 [37]. Highest strengths values are obtained at MnS in the grey iron close to the solubility limit (0.03 - 0.05 ± 0.01).

The ratio of tensile strength to hardness was reported in the study of Gundlach *et al*., 2014 as a measure of quality and size of the flake graphite structure. As the graphite structure becomes more refined, the UTS/HV ratio increases which are a measure of stable and increased graphite flake size. Figure 10 shows the correlation between UTS/HV and the sulphur composition for all the alloys

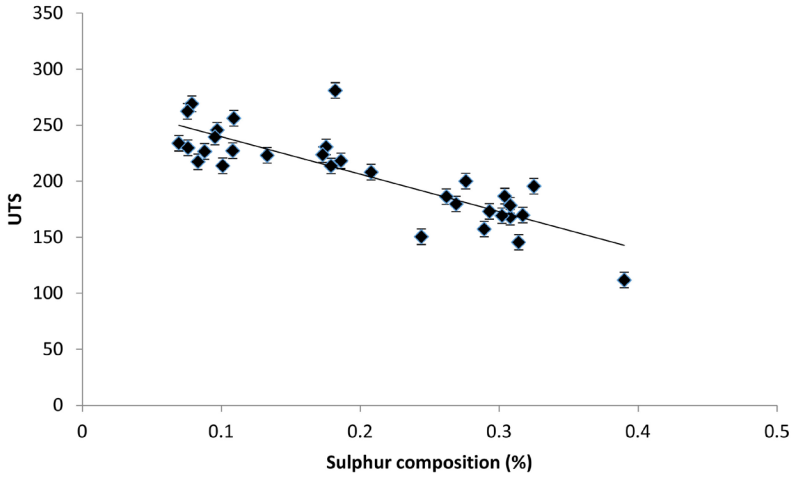

Figure 8. Influence of percentage sulphur content on the ultimate tensile strength.

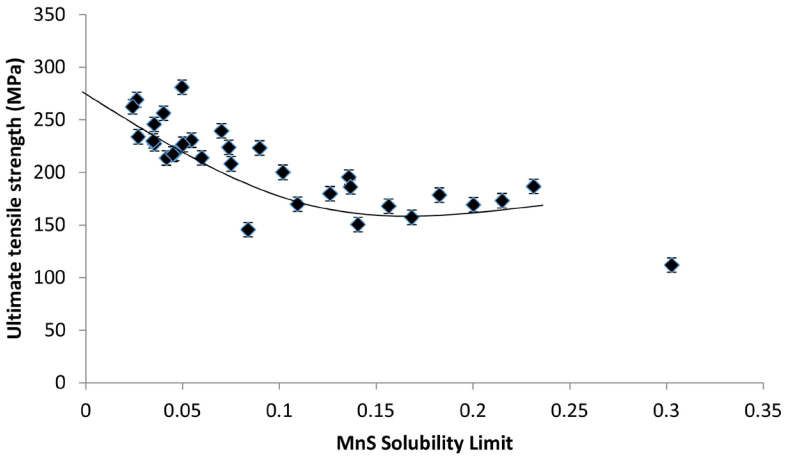

Figure 9. Influence of MnS Solubility on ultimate tensile strength.

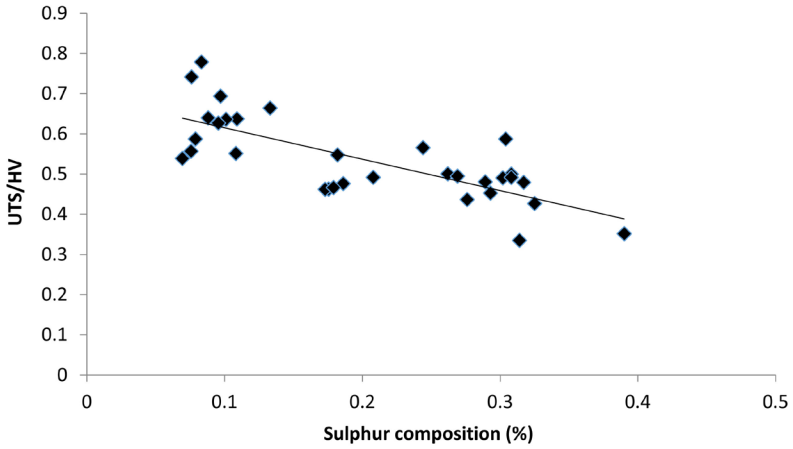

Figure 10. UTS/HV relationship with increased sulphur composition to demonstrated mean flake size.

(And B series). The decrease in the UTS/HV ratio which also is in agreement with the results obtained in Gundlach *et al*., 2015 depicted that the rather reducing UTS/HV is caused by change in the graphite structure which is a function of increasing sulphur content [28] [30]. The convergence of the average flake sizes appears to converge from wider distribution for lower sulphur content. The increase in the sulphur content shows that the fall in UTS/HV value is due to reduction and degenerated graphite flake sizes as observed in the microstructure of the B series alloy.

4. Conclusion

The effect of Cu-Ni and Cu-Ni-Mn addition on the hardness and strength properties and behaviour of hypereutectic grey iron for 32 alloys produced without traditional inoculation route has been investigated in this study. The amount of undercooled graphite formation is dependent on the weight percent addition of Cu and Ni, which acts as graphitizers in the final chemical composition. Graphite formation as observed in the microstructure despite non-inoculation of the as-cast grey iron is due to the increased presence of sulphur with copper and nickel as moderate graphitizers. Predominance of type D graphite in the order of decreased graphitizers resulted in higher degree of undercooling and fewer eutectic cells. The overall increase in the hardness of the alloy produced when compared with similar study in Vadiraj *et al*., 2010 [3] [26] is due to increased carbon content in the alloy. High carbon content in the alloy restrained the forming tendency of silicon and supressed the ferrite forming tendency to produce a fully formed pearlitic matrix. Copper addition is confirmed to promote pearlitic formation and contributes to the hardness amount with increasing Cu content. Copper and nickel additions were also observed to influence the degree of undercooling with fewer eutectics leading to increased type D graphite. Cu-Ni microalloying was also confirmed to promote hardness with the hardening effect limit of nickel observed at 1.3% composition increased level of hardness is also

due to the hardening effect of nickel, however, increased addition of nickel in hypereutectic grey iron has no effect beyond 1.3% nickel composition. The addition of manganese was observed to have a reverse effect on the hardness of the hypereutectic alloy depending on the sulphur content level. While excess manganese beyond what is required to fix sulphur eliminates free ferrite and promote hardness, excess and free sulphur beyond 0.05% sulphur resulted in lower hardness value. Nickel addition affects the ultimate tensile strength in similar way as the hardness with the UTS reducing beyond 1.5% nickel addition. While strength is expected to improve with manganese addition, free and excess sulphur promotes formation of manganese sulphide beyond the solubility limit of MnS in the microstructure affecting the strength properties of the alloy. Highest strengths values are obtained at MnS in the grey iron close to the solubility limit (0.03 - 0.05 ± 0.01). Using the ratio of UTS/HV as a measure of graphite flake size shows that correlation with the increasing sulphur in the alloy. The fall in tensile strength of the hypereutectic grey iron is accompanied with size and change in the graphite structure. For Cu-Mi-Mn addition, excess and free sulphur in the hypereutectic grey iron results in reverse effect of manganese on strength, hardness, reduced graphite flake size and shape. The maximum addition of manganese that can yield optimum hardness is given by the function Mn ≤ 1.7 * S.

Conflicts of Interest

The authors declare no conflicts of interest regarding the publication of this paper.

References

[1] Xu, W., Ferry, M. and Wang, Y. (2005) Influence of Alloying Elements on as-Cast Microstructure and Strength of Grey Iron. *Materials Science and Engineering-A*, **390**, 326-333. https://doi.org/10.1016/j.msea.2004.08.030

[2] Yin F., Takamori S., Ohsawa Y., Sato A. and Kawahara A. (2001) Mn-Cu-Ni-Fe Damping Alloy with Super Workability and Easiness for Recycle. *Journal of Japan Institute of Metals*, **65**, 607-613. https://doi.org/10.2320/jinstmet1952.65.7_607

[3] Vadiraj, A., Balachandran, G., Kamaraj, M., Gopalakrishna, B. and Rao, D.V. (2010) Mechanical and Wear Behaviour of Alloyed Hypereutectic Grey Cast Iron. *Materials Science and Technology*, **26**, 842-848. https://doi.org/10.1179/026708309X12454008169429

[4] Angus, H.T. (2013) Cast Iron: Physical and Engineering Properties. *Technology and Engineering*, **3**, 1-34.

[5] Sulardjaka, S., Atmaja, S.T., Nugroho, S., Adnan, F. and Cahyono, A.D. (2013) The Effect of Alloy Elements on Fatigue Strength of Grey Cast Iron at Room and High Temperature. *Rotation*, **15**, 23-28.

[6] William, F.S. and Hashemi, J. (2011) Foundations of Materials Science and Engineering. McGraw-Hill Publisher, New York.

[7] Soon, K.B., Idris, M.H., Maroof, M.R., Zakaria, Z.A., Sahudin, S., Hanafiah, M.A. and Ahmad, A.H. (2010) Investigation of Processing Parameter for 'In ladle Treat-

ment' of Ductile Iron Using High Sulphuric Pig Iron. *National Conference in Mechanical Engineering Research*, *FKM Conference Hall*, UMP, Kuantan, Pahang, Malaysia, 363-374.

[8] Morsy, M. and El-Kashif, E. (2014) The Effect of Microstructure on High-Stress Abrasion Resistance of Fe-Cr-C Hardfacing Deposits. *Welding in the World*, **58**, 491-497. https://doi.org/10.1007/s40194-014-0132-0

[9] Kalpakjian, S. and Schmid, S.R. (2014) Manufacturing Engineering and Technology. Testing and Materials Annual, Pearson Publisher, Upper Saddle River, NJ, 193-195.

[10] Stefanescu, D.M. (2015) Science and Engineering of Casting Solidification. Springer, Berlin, 17-23. https://doi.org/10.1007/978-3-319-15693-4

[11] Seidu, S.O. (2014) Effect of Compositional Changes on the Mechanical Behavior of Grey Cast Iron. *Journal of Metallurgical Engineering*, **3**, 92-95. https://doi.org/10.14355/me.2014.0302.05

[12] Jezerski, J. and Bartocha, D. (2007) Properties of Cast Iron Modifying with Inoculants. *Journal of Archiving in Materials and Manufacturing Engineering*, **22**, 25-28.

[13] Srinivasan, M. and Seetharamu, S. (2012) Fracture Toughness of Metal Castings. In: *Science and Technology of Casting Processes*, In-Tech Publishing, London, 287-309. https://doi.org/10.5772/50297

[14] Terheci, M., Manory, R.R. and Hensler, J.H. (1995) The Friction and Wear of Automotive GreyCast Iron under Dry Sliding Conditions Part 2. Friction and Wear—Particle Generation Mechanisms and their Progress with Time. *Wear*, **185**, 119-124. https://doi.org/10.1016/0043-1648(95)06593-8

[15] Vadiraj, A., Balachandran, G., Kamaraj, M. and Kazuya, E. (2011) Mechanical and Wear Behavior of Quenched and Tempered Alloyed Hypereutectic Grey Cast Iron. *Journal of Materials & Design*, **32**, 2438-2443. https://doi.org/10.1016/j.matdes.2010.11.052

[16] Mohrbacher, H. and Zhai, Q. (2011) Niobium Alloying in Grey Cast Iron for Vehicle Brake Discs. *Materials Science and Technology Conference and Exhibition* 2011, MS & T11.

[17] Wenbin, Z., Hongbo, Z., Dengke, Z., Hongxing, Z., Qin, H. and Qijie, Z. (2011) Niobium Alloying Effect in High Carbon Equivalent Grey Cast Iron. *Research & Development*, **8**, 36-40.

[18] Chisamera, M., Riposan, I., Stan, S., Militaru, C., Anton, I. and Barstow, M. (2012) Inoculated Slightly Hypereutectic Grey Cast Irons. *Journal of Materials Engineering and Performance*, **21**, 331-338. https://doi.org/10.1007/s11665-011-9907-2

[19] Riposan, I., Chisamera, M., Stan, S., Costache, G. and Barstow, M. (2010) A Comparison of Mould and Ladle Inoculation Treatments of Low Sulphur Hyper-and-Hypoeutectic Grey Cast Irons. *Proceedings of the* 69*th World Foundry Congress*, Hangzhou, 16-20 October 2010.

[20] Lerner, Y. (2003) Titanium in the Rapidly Cooled Hypereutectic Grey Iron. *Journal of Materials Engineering and Performance*, **12**, 141-146. https://doi.org/10.1361/105994903770343277

[21] Chisamera, M., Riposan, I., Stan, S., Anton, I. and Barstow, M. (2011) Effects of Iron Powder Addition on the Solidification Behaviour of Hypereutectic Grey Cast Iron. In: *Key Engineering Materials*, Volume 457, Trans Tech Publications, New York, 90-95. https://doi.org/10.4028/www.scientific.net/KEM.457.90

[22] Chisamera, M., Riposan, I., Stan, S. and Barstow, M. (2011) Structure Characteris-

tics of Iron Powder Treated Slightly Hypereutectic Grey Irons. *International Journal of Cast Metals Research*, **24**, 370-377. https://doi.org/10.1179/1743133611Y.0000000010

[23] Riposan, I., Chisamera, M., Stan, S. and Barstow, M. (2011) Improving Chill Control in Iron Powder Treated Slightly Hypereutectic Grey Cast Irons. *China Foundry*, **8**, 228-234.

[24] Urrutia, A., Celentano, D.J., Gunasegaram, D.R. and Deeva, N. (2014) Thermal Microstructural Multiscale Simulation of Solidification and Eutectoid Transformation of Hypereutectic Grey Cast Iron. *Metallurgical and Materials Transactions A*, **45**, 3954-3970. https://doi.org/10.1007/s11661-014-2340-z

[25] Chisamera, M., Riposan, I., Stan, S., Militaru, C. and Barstow, M. (2011) Influence of Iron Powder Addition on the Structure Characteristics of Hypereutectic Grey Cast Iron. In: *Key Engineering Materials*, Volume 457, Trans Tech Publications, New York, 96-101. https://doi.org/10.4028/www.scientific.net/KEM.457.96

[26] Vadiraj, A., Kamaraj, M. and Sreenivasan, V.S. (2012) Influence of Load and Sliding Speed on Friction and Interface Temperature of Hypereutectic Alloyed Grey Cast Iron. *Transactions of the Indian Institute of Metals*, **65**, 289-296. https://doi.org/10.1007/s12666-012-0132-y

[27] Gundlach, R.B. (2014) Influence of Manganese and Sulphur on the Properties of Cast Iron: Part I-Historical Perspective. *AFS Transactions*, **122**, 287-303.

[28] Akinyemi, O.O., Adeboje, T.B. and Aremu, A.A. (2015) Composite Effect of Nickel and Copper on the Characteristics of Grey Cast Iron. *Proceedings of Canadian-American Conference for Academic Disciplines*, **4**, 357-362.

[29] Meyer, M.H., Gundlach, R.B., Williams, D.C. and Winardi, L. (2014) Influence of Manganese and Sulphur on the Properties of Cast Iron Part II-Experimental Design: AspectsofMelting and Pouring. *AFS Transactions*, **122**, 273-278.

[30] Ghoreshy, M., Zehtab, M. and Kondic, V. (1980) Primary Austenite Dendrites in Grey Cast Irons. *The British Foundryman*, **75**, 277-280.

[31] Gundlach, R., Meyer, M. and Winardi, L. (2015) Influence of Mn and S on the Properties of Cast Iron Part III: Testing and Analysis. *International Journal of Metalcasting*, **9**, 69-82. https://doi.org/10.1007/BF03355617

[32] Sekowski, K., Piaskowski, J. and Wojtowicz, Z. (1972) Atlas of the Standard Microstructures of Foundry Alloys. WNT Warszawa, Poland, 54-55+74-77.

[33] Elkem (2013) Graphite Structures in Cast Irons. Elkem Posters ASA Foundry Product Division.

[34] Fras, E. and Górny, M. (2012) An Inoculation Phenomenon in Cast Iron. *Archives of Metallurgy and Materials*, **57**, 767-777. https://doi.org/10.2478/v10172-012-0084-6

[35] Ruff, G.F. and Wallace, J.F. (1976) Control of Graphite Structure and Its Effect on Mechanical Properties of Grey Iron. *AFS Transactions*, **84**, 705-728.

[36] Bihari, B., Kumar, R. and Singh, A.K. (2014) Effect on the Mechanical Properties of Grey Cast Iron with Variation of Copper and Molybdenum as Alloying Elements. *International Journal of Engineering*, **3**, 121-125.

[37] Alderson, A. (1985) The Influence of Manganese and Sulphur on the Structure and Mechanical Properties of Grey Cast Iron. *The British Foundryman*, **78**, 335-341.

[38] Meyer, M.H., Gundlach, R.B., Williams, D.C. and Winardi, L. (2014) Influence of Mn and S on the Properties of Cast Iron Part II: Experimental Design: Aspects of

Melting and Pouring. *AFS Transactions*, **122**, 273-278.

[39] Mampaey, F. (1981) The Manganese: Sulphur Ratio in Grey Iron. *Fonderie Belgique*, **51**, 11-25.